The Journal of Adhesion, 85:18–54, 2009

ISSN: 0021-8464 print/1545-5823 online
DOI: 10.1080/00218460902727381

Taylor & Francis
Taylor & Francis Group

Fine Tuning the Adhesive Properties of a Soft Nanostructured Adhesive with Rheological Measurements

F. Deplace[1], C. Carelli[1], S. Mariot[1], H. Retsos[1], A. Chateauminois[1], K. Ouzineb[2], and C. Creton[1]
[1]Laboratoire de Physico-Chimie des Polymères et des Milieux Dispersés, UMR, UPMC, CNRS-ESPCI, Paris, France
[2]Research and Technology Cytec Surface Specialties, Drogenbos, Belgium

The major objective of this article is to present recent advances in the methodology to fine tune the adhesive performance of a PSA. In addition to the so-called Dahlquist criterion requiring a low modulus, we propose two additional rheological predictors of the adhesive properties. The first one is derived from the description of the detachment of a linear elastic layer from a rigid substrate. We made an approximate extension of this analysis to the viscoelastic regime and showed that the transition from interfacial cracks to cavitation and fibrillation can be quantitatively predicted from the easily measurable ratio $\tan(\delta)/G'(\omega)$. If a fibrillar structure is formed, the nonlinear large strain properties become important. We showed that the ability of the fibrils to be stretched before final debonding can be predicted from the analysis of simple tensile tests. The softening, which occurs at intermediate strains, and, more importantly, the hardening which occurs at large strains, can be used to predict the mode of failure and the energy of adhesion. The use of this methodology to tune the PSA structure for a specific application has been illustrated for the special case of wb-PSA made of core-shell particles, and improved adhesive properties on polyethylene surfaces have been obtained.

Keywords: Adhesion predictors; Linear viscoelastic properties; Microstructure-property relationship; Nonlinear elasticity; PSA

Received 28 July 2008; in final form 24 November 2008.
Address correspondence to C. Creton, Laboratoire de Physico-Chimie des Polymères et des Milieux Dispersés, UMR 7615, UPMC, CNRS-ESPCI, 10, Rue Vacquelin, F-75231 Paris, Cédex 05, France. E-mail: costantino.creton@espci.fr

1. INTRODUCTION

Pressure-sensitive adhesives (PSA) are soft polymeric materials displaying an instantaneous adhesion on most surfaces upon application of a light pressure [1]. Although the function appears relatively simple, the design of proper PSAs is complex and relies heavily either on polymer chemistry (for acrylic polymers and silicone polymers) or on formulation (for block copolymers and natural rubber) [2].

Although specific requirements for different applications vary, three basic properties have to be optimized for each PSA: peel adhesion, shear resistance and tack. An optimal balance between peel strength and shear holding power is, in particular, required. This balance means that the PSA must be able to dissipate energy during the peeling process (a property optimized for a highly viscous liquid) but be resistant to creep in shear (optimum for solids). In the family of acrylic polymers widely used for PSA, striking this balance means choosing the right monomer composition and the right molecular weight distribution and level of crosslinking. The effect of several molecular parameters of the core polymer such as monomer composition, molecular weight (M_w), molecular weight distribution (MWD), molecular weight between entanglements (M_e), and molecular weight between crosslinks (M_c) on adhesive performance of PSAs have been previously studied [3,4] [5–8] and have shown that the final properties of a PSA are crucially dependent on the balance between crosslinking (imparting cohesive strength) and viscoelastic dissipation (providing a high peel force).

For the specific case of an acrylic core polymer, PSAs are generally weakly crosslinked copolymers of a blend of monomers chosen to adjust the T_g which have an insoluble fraction (gel) and soluble fraction (sol). Increasing the gel fraction, reducing its M_c, and reducing the M_e or increasing the M_w of the sol fraction leads to an increase in resistance to shear. However, peel strength is controlled by the formation and growth of fibrils and is mainly influenced by dissipative processes and flow of polymer chains. Energy dissipation is favored by a low gel content, a sol fraction containing a larger proportion of short chains, and a network with dangling ends [2,9]. Thus, contradictory requirements have to be covered to optimize both shear resistance and peel strength. A very broad molecular weight distribution combined with a highly dissipative sol fraction and a cohesive network formed by the gel is a good and relatively easy way to achieve a practical solution, but has limitations due to the impossibility to control independently sol and gel parameters during the synthesis.

Recent environmental concerns have pushed many industries, particularly in Europe, to develop PSAs made from polymer no longer synthesized in solution but in emulsion in water. In this case, individual particles are being synthesized and the material is then formed by the coalescence of these particles into a homogeneous film. Since the particle grows radially during the synthesis, by absorbing more monomer from the water phase, its radial composition can be controlled by changing the monomer composition during the synthesis and core-shell particles can be easily obtained. These core-shell particles should be distinguished from the usual particles where the more hydrophilic monomers always locate on the outside of the particle and impart more cohesion. This composite structure is used in a number of industrial applications of latexes such as paints and coatings [10].

The objective for PSA is to impart a better shear resistance with a cohesive shell while retaining peel performance with a soft and dissipative core. Thus, shear and peel can be independently tuned since core and shell are synthesized in two distinct steps.

The influence of particle morphology on adhesive performance has already been studied by Aymonier *et al*. [11–13]. However, no special effort to control molecular weight and gel fraction of both phases was made and, in that case, not much improvement was obtained using a heterogeneous morphology or a gradient composition compared with a homogeneous one. The heterogeneous structure of Aymonier *et al*. [12] shows, for example, a lack of adhesion and cohesion probably because the composition of each phase, outer and within the particle, is not optimized for this type of structure.

Our research started from the same idea as the Aymonier-Papon study but we focused on the synergy between particle structure and polymer structure which needs to be optimized globally in order to see an improvement in macroscopic adhesive properties. Our recent experimental results showed that linear viscoelastic properties and nonlinear properties both play fundamental roles in the debonding of the adhesive layer from a substrate [5,14,15]. Yet currently applied methodologies focus too much on simple correlations between end-use properties and linear viscoelastic properties [7,16] and the mechanistic models remain either too complex to use for real materials or neglect large strain properties. We have proceeded in a two step fashion: We present first in Part 2 an improved but simple theoretical description of the debonding mechanisms including both linear viscoelasticity and large strain behavior and we then use existing molecular models of the rheological properties to guide the design of the PSA for the required application. Part 3 contains the materials and

techniques description and Part 4 contains our analyzed experimental results for several core-shell structures of particles.

2. THEORETICAL BACKGROUND

2.1. Tack Experiments

Peeling a soft adhesive layer from a rigid substrate involves rather complex deformation mechanisms [17–20]. These mechanisms, observed in peel tests, have been mostly described and analyzed using axisymmetric probe tests [21] and occur both at the interface between the polymer and the substrate and in the bulk of the material. Relative to the more obvious but more difficult to analyze peel test, the probe test provides a full force–displacement curve and most of the information on the debonding mechanism is hidden in the shape of this curve.

The adhesive performance is typically evaluated quantitatively through three main parameters obtained from the force–displacement curve—the maximal nominal stress, $\sigma_{\max}$, the maximal strain, $\varepsilon_{\max}$, and the adhesion energy, W_{adh}, which is defined as the area under the stress *vs*. strain probe tack curve:

$$W_{adh} = h_0 \int_0^{\varepsilon max} \sigma(\varepsilon) d\varepsilon \tag{1}$$

with h_0 the initial thickness of the adhesive layer and $\varepsilon_{\max}$ the failure deformation corresponding to the detachment of the adhesive from the probe or to the failure of the polymer in its bulk. Caution needs to be taken in the case of cohesive debonding when no failure occurs before the end of the test.

Four types of stress-strain curves have been observed from investigations of a great number of polymers [21–24]. The first type of curve [Fig. 1(a)] is characterized by a sharp maximum at rather low strains and a very small area under the stress-strain curve. At the other extreme (Figure 1c) is the case of a highly viscous liquid [25]. The adhesive joint breaks by cohesive fracture within the adhesive and the debonding process is governed by viscous flow. This is a typical "liquid-like" debonding, also called "cohesive debonding", where some residues of adhesive are left on the probe at the end of the test. In between these two cases, stress-strain curves are characterized by a maximum in the stress followed by a pronounced shoulder [Fig. 1(b-1)]. The curve finally ends up by a decrease in the force to zero. Detachment in that case occurs at the interface between the probe and the adhesive layer. Such a debonding is called "adhesive debonding" (no macroscopic residue on the probe at the end of the

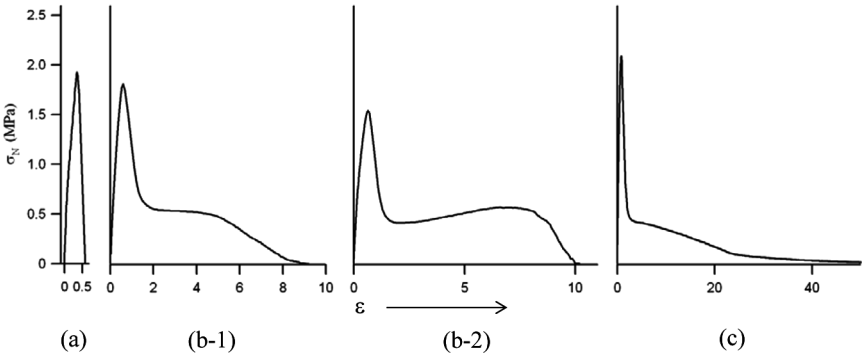

FIGURE 1 Different stress-strain tack curves. (a) Brittle failure; (b) adhesive debonding, with hardening in the case of b-2; (c) cohesive debonding liquid-like behavior.

test). Fig. 1(b-2) is observed when the material strain-hardens just before the final detachment. In that case a slight increase in the stress is observed and a second peak is observed.

2.2. Prediction of Debonding Mechanisms from Linear Rheological Properties

For many scientists working in adhesion science and, in particular, on PSA, it has been tempting to predict adhesive properties from linear viscoelastic properties which are rather simple to characterize with a standard instrument [16,18,26,27]. Yet, rather complex microscopic deformation mechanisms are observed during a debonding process: from interfacial failure, where a crack propagates at the interface, to cavitation or bulk fingering followed by fibrillation, where larger deformations of the adhesive are achieved [21], and it is often not clear what can be predicted from linear viscoelasticity and what cannot. Two criteria based on linear viscoelastic properties are important necessary conditions to obtain PSA properties.

The first one is the so-called Dahlquist criterion [28]: it stipulates that the shear elastic modulus (G') at the bonding frequency must be lower than 0.1 MPa for the layer to be able to form a good contact within the contact time. If the PSA has an elastic modulus which lies in the range defined by Dahlquist, the debonding process is then determined by the coupling of bulk and interfacial properties of the material. Within the framework of linear elasticity, the growth of a defect initially present at the interface is governed by the competition between two different mechanisms: the interfacial growth of a crack,

which is governed by the critical energy-release rate, $\mathcal{G}_c$, and the bulk deformation, determined by the average stress within the layer, and essentially controlled by the elastic modulus of the adhesive, E. The physical principles for this analysis are based on the competition between linear elastic fracture mechanics and cavitation [29,30].

Webber *et al*. [31] showed that for elastic layers, $\mathcal{G}_c/E$ could be used as a predictor of the displacement applied to the adhesive before final detachment. This length scale needs to be compared with two important length scales of the problem: the thickness of the adhesive layer, h, and the size, r, of an initially present interfacial defect (an air bubble, for example) which is typically submicronic (Fig. 2).

The theory predicts that if $\mathcal{G}_c/E$ is smaller than r (Fig. 3a), only interfacial crack propagation is observed and the propagation of the interfacial crack is controlled and limited by $\mathcal{G}_c$. At the other extreme, if $\mathcal{G}_c/E$ is larger than h (Fig. 3b), nonlinear deformation occurs in the bulk, the linear model cannot be used anymore; and a fibril structure is observed. In the intermediate regime, as $\mathcal{G}_c/E$ increases, a transition occurs from interfacial crack propagation to bulk deformation and this has been described in detail with a model silicone adhesive system [14].

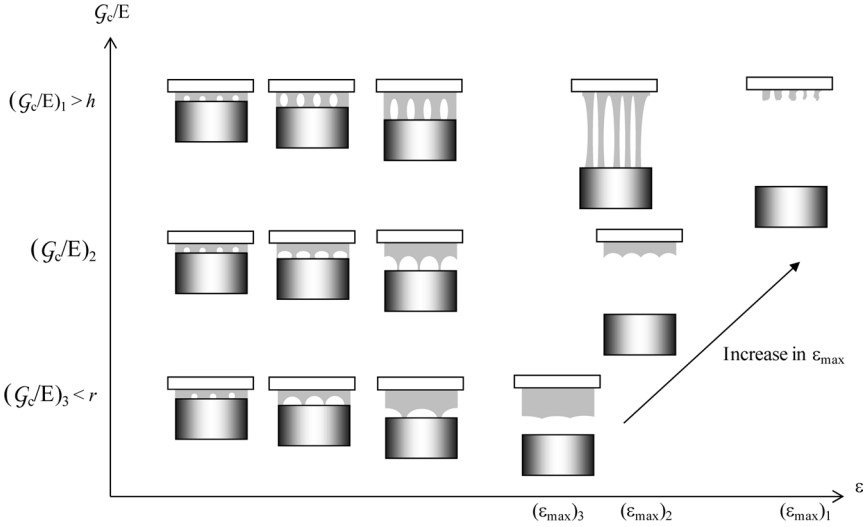

FIGURE 2 Schematics of the debonding process involved during probe tack test depending on the value of the ratio $\mathcal{G}_c/E$. Three different typical cases are displayed. For each value of $\mathcal{G}_c/E$ four or five different steps observed during the test are displayed. (A test can be followed from the left to the right).

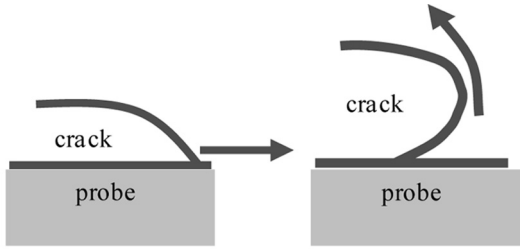

FIGURE 3 Schematic of a crack at the interface between the probe and the adhesive layer. (a) Case of a low value of $\mathcal{G}_c/E$, the propagation of the crack is controlled by $\mathcal{G}_c$; (b) Case of high value of $\mathcal{G}_c/E$, bulk debonding is limited by E.

This elastic approach assumes that the layer is linearly elastic and that dissipative properties are confined in a small volume very close to the propagating crack. For soft and viscoelastic PSAs this is clearly incorrect. However, an extension of the model to linear viscoelasticity can be considered.

For a crack propagating at the interface between a rubbery material and a solid surface, $\mathcal{G}_c$ can be written as:

$$\mathcal{G}_c = \mathcal{G}_0(1 + \phi(a_T V)), \tag{2}$$

where $\mathcal{G}$ is the resistance to crack propagation at vanishingly low crack velocity and $\phi(a_T V)$ is the dissipative factor.

This dissipative factor is related to the viscous dissipative properties of the adhesive but generally not in an obvious manner [32]. However, Maugis and Barquins have shown that for simple elastomers and relatively weak adhesion due to van der Waals forces alone, one can approximate [33]:

$$\phi(a_T V) = k \ \tan\delta(\omega), \tag{3}$$

where k is a constant to be determined by experiment.

While this is clearly a crude approximation, it has been qualitatively confirmed by Saulnier *et al.* [34] who studied theoretically the adhesion of a linear viscoelastic material on a solid surface [33]. The Young's modulus, E, of the elastic model can be replaced by the frequency dependent elastic component of the shear elastic modulus, $G'(\omega)$. Therefore, in the viscoelastic case, one can write:

$$\frac{\mathcal{G}_0}{E} \approx \frac{\mathcal{G}_0(1 + \phi(a_T V))}{G'(\omega)} = \frac{\mathcal{G}_0(1 + k\tan\delta(\omega))}{G'(\omega)} \approx k\frac{\mathcal{G}_0 \tan\delta(\omega)}{G'(\omega)}. \tag{4}$$

The implication of this result is that if the experimental geometry and the surface of the substrate are kept constant, the ratio $\tan \delta(\omega)/G'(\omega)$ experimentally obtained from linear rheological measurements should play the same role as $\mathcal{G}_c/E$ in the linear elastic model.

Using $\tan \delta(\omega)/G'(\omega)$ is clearly an approximation and requires an assumption on the value of ω but it has the advantage to be easily measured by widely used techniques. In real probe tack experiments the strain rates in the adhesive layer are heterogeneous spatially and temporally, so ω can only be an approximate value and we propose to use the value $2\pi V_{deb}/h_0$, where V_{deb} is the velocity of the probe and h_0 is the initial thickness of the layer, as an estimate of ω.

From this approach, one can establish a quantitative criterion for the formation, or not, of fibrils using only results obtained from rheological measurements in the linear regime. Following the approach of the elastic theory there should be a transition in mechanism from interfacial propagation of a crack to cavitation at a given value of $\tan \delta(\omega)/G'(\omega)$. However, the value of $\tan \delta(\omega)/G'(\omega)$, at which the transition occurs, will depend on $\mathcal{G}_0$ of the probe-adhesive interface-and, from Eq. (4), will increase as $\mathcal{G}_0$ decreases. As shown on the deformation map in Fig. 4, one can, for example, predict a lower critical value on a stainless steel surface $(\tan(\delta)/G')_c$, stainless steel than on a polyethylene (PE) surface, $(\tan(\delta)/G')_{c,PE}$. However,

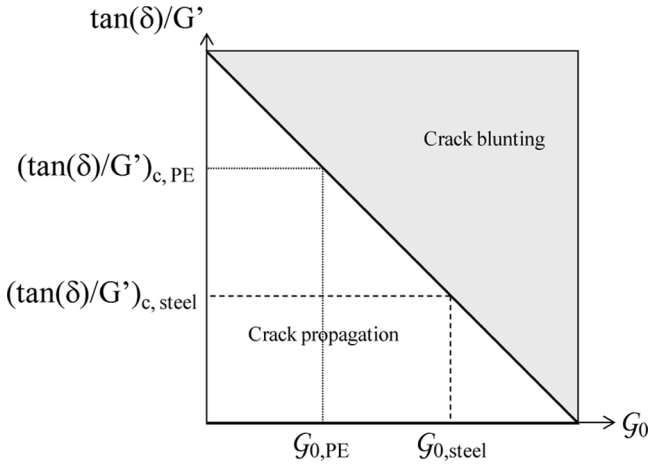

FIGURE 4 Prediction of a transition from interfacial propagation of a crack to cavitation from $\tan(\delta)/G'$ values. Critical value of $\tan(\delta)/G'$ depends on work of adhesion of the probe-adhesive interface, $\mathcal{G}_0$.

because k in Eq. (4) is unknown, the transition point can only be obtained from experimental results and can provide guidance when designing PSAs. This will be done in Section 4.

The limits of the linear viscoelastic approximation to design PSAs is obvious if one considers larger values of $\tan(\delta)/G'$. If the PSA becomes a liquid, dissipation increases dramatically and, of course, the modulus $G'(\omega)$ decreases well below the Dahlquist criterion. This leads to the prediction that viscous fluids will be tacky on almost any surface and this is borne out by experiments. However, PSAs are required to resist creep and as such cannot be liquids. A third criterion addressing this aspect must therefore be defined.

2.3. Prediction of Debonding Mechanisms from Nonlinear Rheological Properties

As discussed previously, if $\mathcal{G}_c/E$ is larger than the initial thickness of the layer or, for a given surface, if $\tan\delta(\omega)/G'(\omega)$ is larger than a critical value, bulk growth of the cavities is favored and foam is formed as the walls between cavities are extended into fibrils. At higher strains corresponding to the fibrillation regime, the behavior of the adhesive is dominated by a competition between viscoelastic extension of the cavity walls and the detachment of the fibrils from the probe [35]. During the fibrillation process, once the fibrils are formed, the only possible option in the absence of strain hardening is the thinning of the central section of the fibril, which results in eventual cohesive failure [21]. This kind of behavior is, for example, foreseeable in the case of a viscoelastic liquid characterized by the progressive decrease of its reduced stress as the deformation increases.

If the material is crosslinked even slightly, a part of external work energy is elastically stored in the fibrils [36]. An adhesive failure is expected and the fibrils will peel off from the probe as soon as either the stored energy in the filaments is high enough to overcome the adhesion energy [37] or the stress in the fibril is high enough to overcome the surface forces (the two cases are not easy to distinguish experimentally). The higher the amount of elastic energy stored the earlier the detachment occurs. High adhesion energy and high maximal deformation of the fibrils can be reached only if elongation of the fibrils is accompanied by some energy dissipation. Energy can be dissipated, for example, through the relaxation of polymer chains during the extension. Stress *vs.* strain and reduced stress *vs.* $1/\lambda$ tensile curves are useful in that case since for a weakly entangled system a pronounced softening is an indication of a pronounced viscoelastic behavior [35,38].

Tensile experiments can then be used as a tool to investigate the large strain behavior of the material [5,39,40]. An example of nonlinear behavior is shown on the stress-strain tensile curve displayed in Fig. 5. One can observe a pronounced softening at intermediate strains followed by a hardening at large strains.

The intrinsic nonlinear behavior of PSAs appears more clearly using the Mooney stress, σ_R, defined as:

$$\sigma_R = \frac{\sigma_N}{\lambda - 1/\lambda^2}. \tag{5}$$

This representation normalizes the measured stress by the predicted behavior of a neo-Hookean rubber in uniaxial extension and is usually plotted as a function of $1/\lambda$. In Fig. 6a, σ_R of two nonlinear elastic solids and a neo-Hookean rubber are displayed. The deviation of the behavior of a material from rubber-like elasticity is quantitatively predicted by the slope of the intermediate part of the reduced stress *vs*. $1/\lambda$ curve. In Fig. 6b, the reduced stress of a viscoelastic solid and the reduced stress of a viscoelastic liquid are displayed. The decrease in reduced stress with increasing extension is due to the concomitant relaxation of the stress by viscoelastic processes and the progressive orientation of the entanglements in the tensile direction as predicted by Rubinstein and Panyukov [41]. The relative importance of these

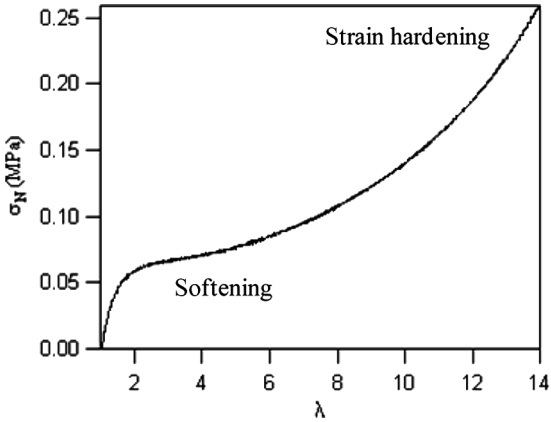

FIGURE 5 Example of a PSA formulation (styrene-isoprene-styrene, SIS, triblock copolymer blended with 42 wt% of diblock. The formulation contains 60 wt% tackifying resin.) with nonlinear elastic properties: softening at intermediate strains, hardening at high strains. The tensile test was performed at a crosshead velocity of 500 mm/min (after [39]).

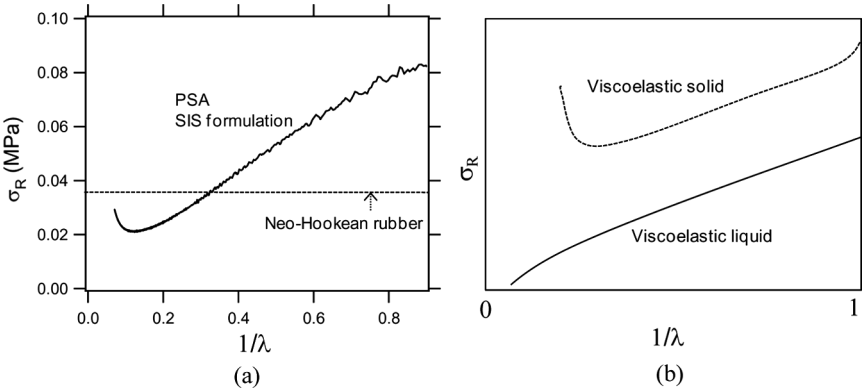

FIGURE 6 Mooney-Rivlin representations of tensile results. (a) Comparison of a PSA (styrene-isoprene-styrene, SIS, triblock copolymer blended with 42 wt% of diblock. The formulation contains 60 wt% tackifying resin) (solid line) with result of a neo Hookean rubber (dotted line); (b) Comparison between a viscoelastic solid (dashed line) and a viscoelastic liquid (solid line). (Schematics of tensile curves are depicted in this plot).

two mechanisms in softening the material can only be addressed by tests performed at different strain rates.

A liquid-like behavior is characterized by the absence of a well defined minimum in this $1/\lambda$ representation and of strain hardening at a high extension ratio (the end of the test corresponds to the left side part of the curve).

In a previous study [5] we suggested fitting the data using the empirical Mooney-Rivlin model which, in uniaxial tension, predicts:

$$\sigma_N = 2\left(C_1 + \frac{C_2}{\lambda}\right)\left(\lambda - \frac{1}{\lambda^2}\right). \tag{6}$$

Two characteristic materials parameters (C_1 and C_2) can be extracted (Fig. 7). C_1 and C_2 can be approximately interpreted as the contribution due to permanent and temporary crosslinks to the modulus, respectively [39].

C_2/C_1 can be used to estimate the contribution of temporary crosslinks compared with that of permanent crosslinks. Very high values of C_2/C_1 were interpreted as a signature of an under-crosslinked material while very low values of C_2/C_1 were obtained for highly crosslinked materials. For homogeneous acrylic copolymers synthesized in solution [5], a value of $C_2/C_1 \sim 5$ was close to the optimum. Lower values typically gave too elastic and well crosslinked materials. This

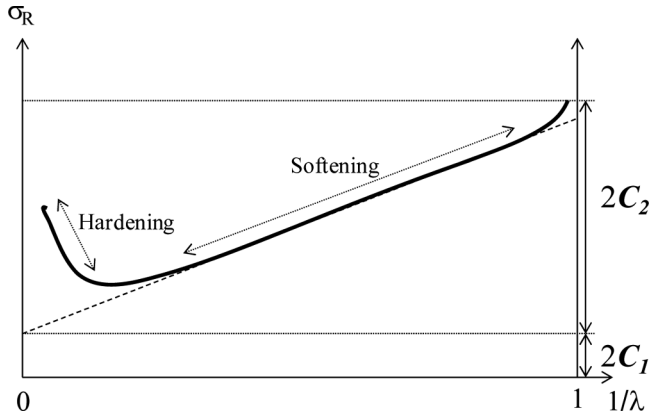

FIGURE 7 Mooney-Rivlin representations of tensile results of a typical PSA. Quantitative estimation of coefficients C_1 and C_2.

approach was, however, developed for relatively cohesive PSAs for permanent applications. Some very soft PSAs can have negative values of C_1 as defined in Fig. 7 so a more general methodology needs to be developed. The important point here is that the σ_R *vs.* $1/\lambda$ curve should have a well-defined minimum for the approach to be meaningful and this will be discussed in Section 4.

As a conclusion, the third criterion for the PSA design is the existence of a well-defined minimum in the σ_R *vs.* $1/\lambda$ curve and a ratio of $C_2/C_1 > 5$ with exact values depending on applications.

3. EXPERIMENTAL SECTION

3.1. Materials

The model PSA latexes used in this study were synthesized by a semi-continuous emulsion polymerization process initiated by ammonium persulfate. Latex particle stability is controlled by a combination of anionic surfactants (2 wt% of the total monomer content). Na_2CO_3 is used as a buffer. Polymerizations were carried out in a 3 l glass reactor equipped with a reflux condenser and anchor stirrer. The temperature was controlled through the circulation of water from a thermostatic bath in the reactor jacket. The latex solid content was determined gravimetrically and lay between 50 and 55 wt%. The average particle diameter was found to be equal to about 250 nm (measurements were performed with quasi-elastic light scattering, Nicomp^{TM}, 380 ZLS, Santa Barbara, CA, USA).

The latexes were made from random copolymers of butyl acrylate (BA) glass transition temperatures [42] of the homopolymer ($T_g = -54°C$), 2-ethyl hexyl acrylate (2-EHA) ($T_g = -50°C$), ethyl acrylate (EA) ($T_g = -24°C$), methyl methacylate (MMA) ($T_g = 105°C$, for the atactic), acrylic acid (AA) ($T_g = 106°C$), and styrene (S) ($T_g = 100°C$) as the main monomers. The monomer composition varies from one latex to another and is used to adjust the glass transition temperature. Since this paper focuses more on the relationship between rheological properties and adhesive properties, we will not disclose the exact monomer composition for each latex but simply the details necessary to follow the arguments.

Experimental results have been obtained on particles with a core-shell morphology which are prepared by using two-step, seeded, semi-continuous emulsion polymerization. This particular morphology of the particles was chosen in order to create a stiff and elastic connected network of shells in a soft and dissipative matrix in the fully dry film.

The structure of the film can be characterized by Atomic Force Microscopy (AFM) in tapping mode following the methodology developed by Mallégol *et al*. [43]. Although, for all films, AFM pictures clearly show that the memory of the shape of the particle is retained and an example is shown in Fig. 8, it is difficult to prove that a real core-shell structure, as depicted in Fig. 9, actually exists in the film.

The theoretical honeycomb-like structure is displayed in Fig. 9. Ideally, the cohesion and shear resistance should then be controlled

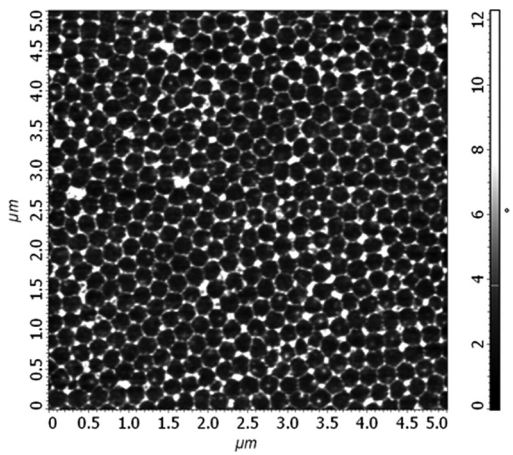

FIGURE 8 Phase AFM image of a hard shell-soft core particle.

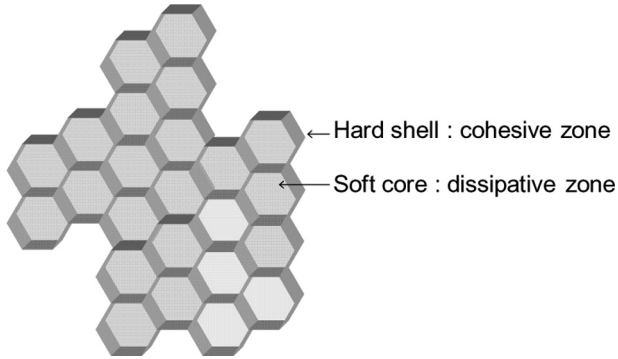

FIGURE 9 Theoretical 3-D honeycomb-like structure obtained after the drying of soft core-hard shell particles.

by properties of the percolating structures of the shells while tackiness should be adjusted by the properties of the core.

The first part of the experimental results section will focus on a series of hard (high T_g) shell-soft (low T_g) core particles. Within the present work, mainly two parameters will be varied: T_g (of both the shell and the core) and the amount of chain transfer agent (CTA) in the core. T_gs have been changed through the monomer composition. Specific values of variable parameters are summarized in Table 1. Adhesive performance of these heterogeneous materials will be compared with that of a film made from particles synthesized by using a one-step polymerization. This film will be considered as a benchmark and called WB. It should be noted that WB as well retains the memory of the shape of the particles.

All these particles have a thin shell and are characterized by a core/shell ratio equal to 91/9 (wt%). The diameter of the particles lies

TABLE 1 Some Characteristics of the Hard Shell-Soft Core Particles Studied

	WB	HS1	HS2	HS3	HS4	HS5
Shell T_g (°C)[1]	–	64	64	6.3	6.3	6.3
Core T_g(°C)[1]	–	−60	−45.5	−45.5	−38.3	−33.2
T_g of the adhesive film (°C)[2]	−50	−60	−45	−41.6	−47	−38
%CTA_{core} (%wt/total monomer)	TA1[3]	0	0.013	0.03	0.03	0.1

[1]Shell and core T_gs are calculated using the Fox equation.

[2]The final T_g of the adhesive film is measured by differential scanning calorimetry at a heating rate of 10°C/min.

[3]Value not reported here since it is Cytec proprietary information.

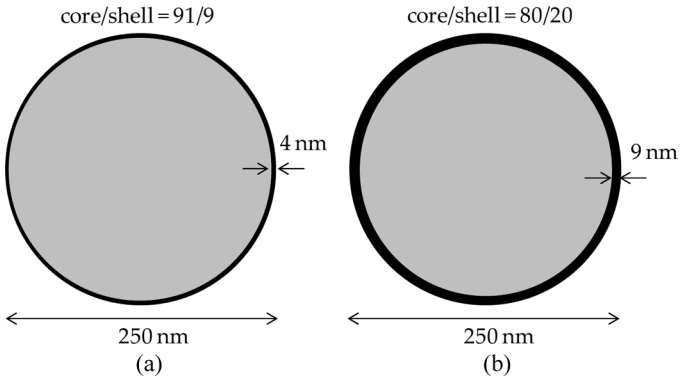

FIGURE 10 Representation of two single particles with the corresponding shell thickness. (a) Core/shell ratio = 91/9; (b) Core/shell ratio = 80/20.

between 205 and 275 nm. A single particle with the corresponding thickness of the shell is represented in Fig. 10.

The second part of the experimental results section will be more focused on soft shell-soft core particles with a core/shell ratio of 80/20 (Table 2). A single particle with the corresponding thickness of the shell is represented on Fig. 10. They are characterized by almost the same monomer composition in both the shell and the core, except that the amount of chain transfer agent added is a little lower (0.037 wt%/total monomer of the shell) in the shell and that the shell contains some diacetone acrylamide (DAAM) groups (2 wt% total monomer of the shell). The crosslinking reaction of these groups can be activated if adipic acid dihydrazide (ADH) is added to the water phase just prior to the drying of the latex. The two materials studied (SS1 and SS2 in Table 2) are nearly the same. In both cases, the gel content of the core is equal to zero as a consequence of the high amount of CTA. The amount of CTA is, however, slightly lower in SS2. These two series of latexes have been chosen as examples to illustrate the methodology used to design the best particle structure.

TABLE 2 Some Characteristics of Soft Shell-Soft Core Particles Studied

	WB	SS1	SS2
Shell T_g (°C)[1]	–	−41	−41
Core T_g(°C)[1]	−50	−41	−41
Gel content	58.3	0	0
% CTA_{core} (%wt/total monomer)	TA1	0.12	0.08

[1] T_gs are calculated using the Fox equation.

3.2. Experimental Techniques

Linear and nonlinear viscoelastic properties both play fundamental roles in the debonding of the flat probe from the adhesive layer during probe tack experiments. A better understanding of the mechanisms involved during probe tack experiments can be achieved through the decomposition into linear and nonlinear properties. This is obtained by performing some rheological measurements at small strain and tensile experiments at large strain, using a simpler geometry compared with the probe tack geometry.

3.2.1. Sample Preparation

For tack and rheological experiments, a small amount of latex was deposited at one end of a precleaned microscope glass slide. A doctor blade with a gap of 300 or 400 μm was used to spread the emulsion. Once the films were spread they were allowed to dry in air at room temperature and ambient humidity about ten hours. At the end of this first drying step, the layers were transparent. These films were then dried in an oven at 110°C for 5 min at atmospheric pressure. The resulting films had thicknesses of approximately 100 μm.

For tensile experiments, samples were prepared in silicone molds. Latexes were allowed to dry in air about ten days at room temperature and ambient humidity. They were then dried at 110°C for 5 min at atmospheric pressure. The resulting films had thicknesses of approximately 800 μm.

3.2.2. Tack Experiments

Probe tack experiments were performed on our custom-designed probe tester allowing the simultaneous observation of the debonding process through the transparent glass substrate. A schematic of the test geometry is shown in Fig. 11 and further details on the experimental setup can be found elsewhere [24]. A typical experiment was carried out as follows: the flat-ended probe was brought in contact with the adhesive layer at a constant probe velocity until a set compressive force was reached, kept at a fixed position for a given time, and subsequently removed at a constant probe velocity. For each experiment the maximum area of the contact during the compression stage was determined from the video observation. The experimental force-displacement curve was transformed into a nominal stress-strain curve by dividing the force by the maximum contact and the displacement by the initial thickness of the adhesive layer (by convention the displacement is zero when the force becomes tensile). In addition, strain calculations took into account the compliance of the setup,

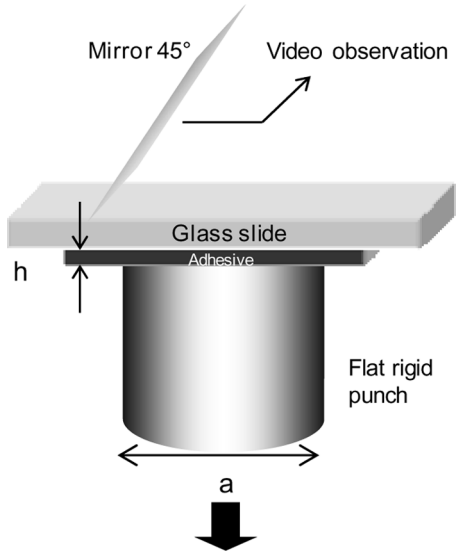

FIGURE 11 Schematic of the geometry of the probe tack test.

which includes the bending of the glass slide, so that the stress-strain curve reflects solely the deformation of the adhesive layer. Certain parameters were kept constant for the present study. Tack experiments were all performed at room temperature and with a compressive force of 70 N (corresponding to an average pressure of 1 MPa for a probe fully in contact). The contact time was set at 1s, and the approach velocity (compressive stage) was set at 30 μm/s. The debonding velocity was varied between 10 and 1000 μm/s. If a sufficient constant compressive pressure is applied on the layer and if the storage modulus of the layer at 1 Hz is below about 0.1 MPa, the compressive stage has little effect on the tensile results. However, the conditions of the compression stage were kept constant when testing a series of adhesives.

The choice of stainless steel as a standard probe surface was dictated by convenience. To test different surfaces, a probe coated with high density polyethylene (PE) was also used. Since surface roughness can affect probe test results [44,45], the degree of surface roughness was well controlled in the case of stainless steel surfaces. The flat ends of the probes were first polished with several grades of abrasive paper until a final average roughness of 0.1 μm as measured with an optical profilometer. Plates of PE were used as received. Unlike steel surfaces, PE surfaces were not polished for this

work. However, some complementary measurements were performed on PE surfaces polished following the same procedure as the one used for steel surfaces and results showed only a slight decrease in the magnitude of the stress of the peak compared with the non-polished PE surfaces. The same probe was used throughout a series of tests and its flat end was cleaned with water and acetone in the case of stainless steel and ethyl acetate in the case of PE.

3.2.3. Small Strain Viscoelastic Properties

Performance of PSAs is highly related to their linear viscoelastic properties. Dynamic mechanical properties have been investigated using a newly designed microrheometer [46]. The system is based on a sphere-on-flat contact configuration (Fig. 12). The sapphire lens in normal contact with the film is allowed to rotate about an axis parallel to the specimen surface. The rotation axis passes through the center of the virtual sphere defined by the lens, so that the tangential movement can be assimilated to a lateral displacement of the sphere. The tangential stiffness associated with the flexible springs of the microrheometer is 0.25 mN/μm and was negligible compared with the stiffness of the samples studied.

During the tests, the contact between the lens and the layer is made by applying a normal displacement to the lens. A normal force, P, in the range of 0–2 N results from this contact. The lens is then actuated by a piezoelectric actuator (maximal displacement=90 μm) which is operated in closed loop control using the signal of a non-contact displacement transducer (optical fibre) as an input. The tangential load is

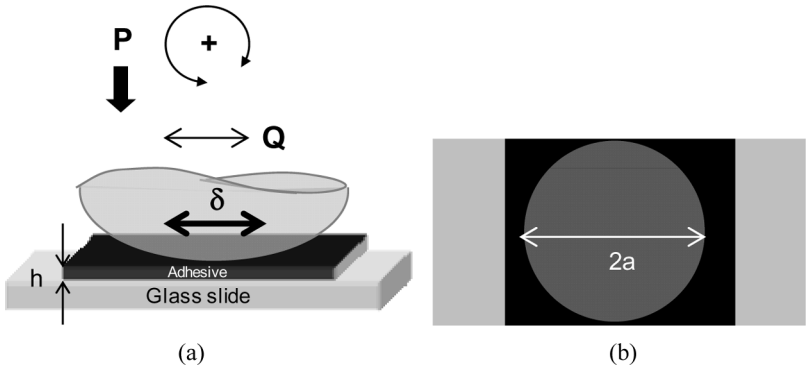

FIGURE 12 (Left) Sphere on flat configuration of the microrheometer used to measure linear viscoelastic properties of adhesive layer. (Right) Top view of the contact between the sphere and the layer.

continuously monitored using a piezoelectric load cell (with a maximal load of 50 N and a resolution of few millinewtons) with an extended dynamic range (from 10^{-2} to 10^{3} Hz).

Rheological tests were performed at a small displacement amplitude (imposed shear strain $\gamma < 0.08$) using a sinusoidal displacement signal at a frequency between 0.1 and 10 Hz. These tests are aimed at providing an estimate of the commonly used rheological properties [storage modulus G', dissipative modulus G', and the loss tangent $\tan(\delta)$] of the adhesive layer from the measurement of the dynamic contact stiffness. Using this configuration, results are valid only if no substantial microslip is induced within the contact, and this condition is, in general, verified in the case of adhesive layers. All linear rheological measurements were performed at room temperature. Some results are shown in Fig. 13. The contact mechanical data and the parallel plate data nearly overlay except at high strain rates ($f > 10$ Hz) where $G'_{contact}$ seems to drop down compared with $G'_{rheometer}$. This is an intrinsic limitation of the setup since, above 10 Hz, we draw nearer to the resonant frequency of the system. Thus, we can confidently use the contact mechanical technique to measure rheological properties of

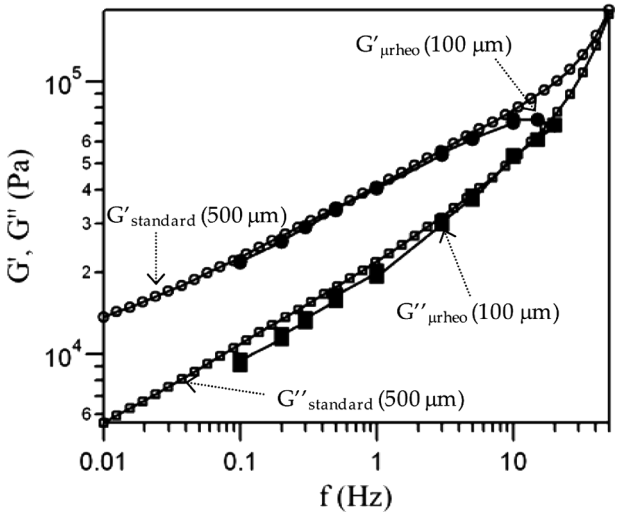

FIGURE 13 Frequency dependence of the storage moduli (G', circles) and loss moduli (G'', squares) for the industrial benchmark PSA based on latex particles made of random copolymers of 2-EHA, EA, MMA, and S (control sample). Filled symbols correspond to data obtained from our contact mechanical test, and open symbols correspond to data obtained from conventional shear rheometry.

thin adhesive layers in a range of frequencies between 0.1 and 10 Hz. The advantage of this technique is its ability to measure G' and G'' of thin supported films down to thicknesses of about 20 μm.

3.2.4. Large Strain Properties: Nonlinear Elastic Properties

Tensile tests were performed on a standard tensile testing machine (JFC TC3, Bordeaux, France) equipped with a Hounsfield non-contacting laser extensometer (Horsham, PA, USA) allowing an accurate measurement of the strain even when the sample slips slightly between the clamps. The crosshead velocity, V_t, was chosen equal to 50 mm/min corresponding to an initial strain rate of about $0.05\,s^{-1}$. All tests were carried out at room temperature. The force (F) and displacement (L) data were directly obtained from the tensile machine. Nominal stress (σ_N) and strain (ε) were then calculated using the initial value of the width, w_0, the thickness, e_0, and the initial distance between the clamps, L_0.

4. RESULTS AND DISCUSSION

4.1. Linear Viscoelastic Properties and Adhesive Properties

As discussed in the Introduction, adhesive tests are complex and difficult to interpret directly in terms of microstructure or molecular structure of the polymer. As stand-alone they can only provide some guidance to the expert or within a given family of materials in the final optimization stage. We present here some examples where the careful analysis of the linear viscoelastic properties can be used to direct the synthesis in the right direction.

4.1.1. Influence of the Elastic Modulus: The PSA Must Be Soft Enough

The first example, where results obtained on HS1 and HS2 are presented, shows how a change in the modulus of the material, obtained here mainly through a change of the T_g of the core (the increase in the CTA content in the core from 0 to 0.013 wt % probably has a negligible effect compared with the change in T_g) can have a profound influence on adhesive properties.

On Fig. 14 are shown both the evolution of the shear elastic modulus as a function of frequency in the linear regime (Fig. 14a) and stress-strain tack curves of the corresponding materials (Fig. 14b). Behavior of core-shell particles characterized by a low core T_g and a high shell T_g is compared with that of a benchmark PSA (WB) made of homogeneous low T_g particles synthesized by using a one-step polymerization.

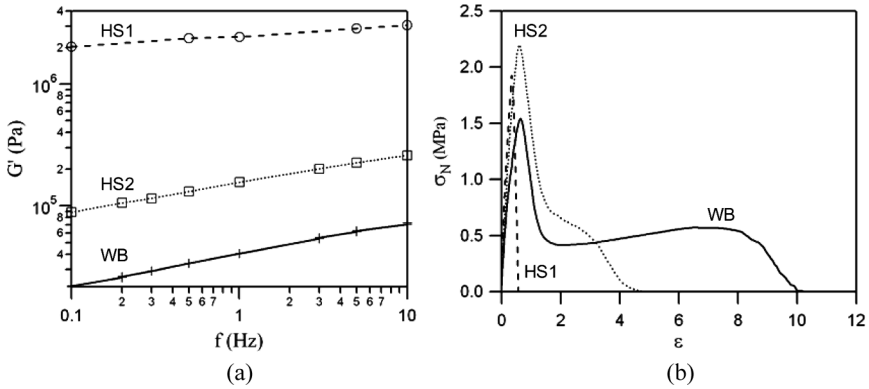

FIGURE 14 (a) Evolution of the elastic modulus with frequency for two hard shell-soft core particles; (b) Stress-strain tack curves. Tests were performed on stainless steel probe at 1000 μm/s. (Dashed line: HS1, dotted line: HS2, solid line: WB.)

As discussed in the theoretical background section, the first requirement for a PSA in terms of linear rheological properties is that the elastic component of the shear modulus should be below 100 kPa. In Fig. 14a, one can observe that $G'(\omega)$ of HS1 is higher than this defined boundary and nearly constant around 2 MPa between 0.1 and 10 Hz. This is clearly too hard to conform to a rough surface and the stress-strain curve of such an adhesive layer in probe tack is characterized by a sharp decrease of the stress without a fibrillation plateau and a very low adhesive energy.

On the other hand, the elastic modulus of WB lies well below 0.1 MPa in the overall range of frequencies studied and that of HS2 does not exceed 0.25 MPa. In these cases, interfacial failure proceeds by cavitation and a fibril structure is formed.

The increase in the T_g of the core from -60 to -45°C leads to a significant decrease in the shear elastic modulus, G'. Intuitively, we would expect an increase in G' with an increase in T_g. The inverse tendency observed here is not easily explained. It may be due to different organizations of the core-shell structure depending on the difference between the T_gs of both phases. In the case of HS1, the resulting modulus is too high for the material to be spontaneously sticky. A careful adjustment of the T_g of the core is necessary.

Our second example is given in Fig. 15. The synthetic strategy here was to decrease the elastic modulus playing with both the T_g of the shell and with the CTA amount in the core. A decrease of the T_g of the shell from 64°C (HS2) to 6.3°C (HS3) was accompanied with an increase in the CTA amount in the core from 0.013 to 0.03 wt%.

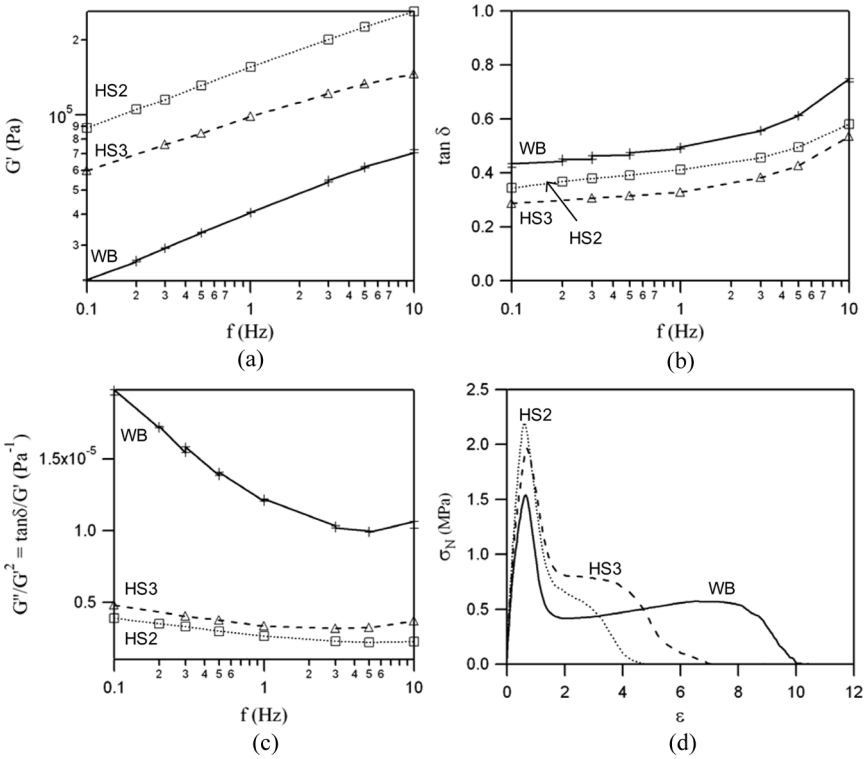

FIGURE 15 Evolution of (a) the elastic modulus; (b) $\tan(\delta)$; and of (c) the ratio $\tan\delta/G'$ with frequency for two hard shell-soft core particles; (d) Stress-strain tack curves. Tack experiments were performed on stainless steel at 1000 μm/s. (Dotted line: HS2, dashed line: HS3, solid line: WB.)

In this case, the elastic modulus values of the materials are in the suitable range for the cavitation process to be complete and the fibrillation process to be activated.

To understand the differences in adhesive properties of Fig. 15d, it is necessary to examine this time the dissipative properties of the latexes and, more specifically, the parameter $\mathcal{G}_c/E$. Once cavities are formed at the interface between the probe and the adhesive film, their rate of propagation is dependent on $\tan\delta(\omega)$. The more difficult is the crack propagation the smaller are the cavities and the higher is the value of $\tan\delta(\omega)$.

As discussed in the theoretical background section, once cavities are fully formed (on the right side of the peak) $\tan\delta(\omega)/G'(\omega)$ can be used as an approximation of $\mathcal{G}_c/E$ for a given surface. The lower is

$\tan\delta(\omega)/G'(\omega)$ the more crack propagation is favored compared with crack blunting and the sooner the detachment is expected to occur. This is what is experimentally observed (Fig. 15c and Fig. 15d). Much shorter fibrillation plateaus are obtained on the probe tests in the case of low values of $\tan\delta(\omega)/G'(\omega)$ ($\tan\delta/G' < 0.5^*/10^{-5}\,\mathrm{Pa}^{-1}$). Let us finally examine a third example where different surfaces are used. Figure 16 shows tack results of HS3 on a stainless steel and a polyethylene (PE) surface. A large decrease in adhesion energy is observed when tests are performed on a low energy surface such as PE. If values of $\tan\delta(\omega)/G'(\omega)$ are high enough for acceptable adhesion energy on stainless steel, a higher value is probably required for better performance on PE. This results from the dependence of $\mathcal{G}_c$ on the surface energy and by the higher critical value of $(\tan\delta/G')_c$ necessary for crack blunting on PE (Fig. 4) than on stainless steel. Such a result clearly demonstrates the need to adapt the linear viscoelastic properties of the PSA to the substrate as discussed recently [14,40]. This shortcoming then requires a change in synthesis strategy.

To conclude, the absolute values of T_g of the soft core and of the hard shell and the amount of CTA in the core have an obvious influence on rheological and adhesive properties of the material. It is also clear that these properties depend on how the two phases are matched. A good compromise in terms of adhesive properties seems to be reached when the T_g of the core equals $-45.5°C$ and the T_g of the shell equals $6.3°C$ with a CTA content in the core of 0.03 wt%. However,

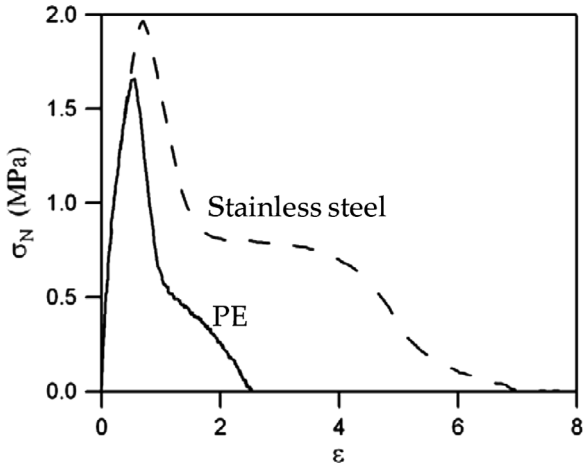

FIGURE 16 Tack stress-strain curves of a HS3. Dashed line: on stainless steel. Solid line: on PE. Experiments were performed at 1000 μm/s.

Fig. 16 shows that adhesive energy on PE is still very low. In order to further improve adhesive properties, the strategy examined in the following section is to try to enhance $\tan\delta(\omega)$ by increasing the amount of CTA in the core.

4.1.2. Influence of the Dissipative Properties: How to Further Increase the Adhesive Energy?

Linear rheological properties of hard shell-soft core particles differing both by their amount of CTA in the core and by their core T_g are displayed in Fig. 17(a). Tack experiments have been also performed with these materials on stainless steel and PE at two speeds of debonding (V_{deb}=10 and 1000 μm/s) (Fig. 17(b)).

As a result of the changes in chemistry it is obvious that HS5 has a higher elastic modulus, G', and is more dissipative, while HS4 is softer and more elastic. Values of $\tan\delta/G'$ can be used to estimate $\mathcal{G}_c/E$. Comparing HS4 and HS5, a crossover of the curves representing values of $\tan\delta/G'$ as a function of the frequency is observed at about 2 Hz. This means that at small frequencies, dissipation seems to dominate, while at higher frequencies, this is most probably bulk properties characterized by elastic modulus which play the major role. Fig. 17b illustrates the fact that the competition between the interfacial propagation of the crack and the vertical extension of the fibrils is governed by $\tan\delta/G'$. For example, at 10 μm/s, on stainless steel, as on PE, the lower value of $\tan\delta/G'$ in the case of HS4 results in a debonding of the layer at a lower nominal strain. At 1000 μm/s, on stainless steel, a longer fibrillation plateau is obtained for HS5 but on PE the tendency is reversed and is more in agreement with the frequency dependence of linear rheological parameters. The high elastic modulus of HS5 is responsible for the low value of $\tan\delta/G'$ at high frequencies and leads to the brittle fracture characterized by the sharp decrease in stress after the initial peak.

As a conclusion for this section concerning the use of linear rheological properties, we showed that trends in tack experiments can be reasonably predicted using linear rheology. A criterion for adhesion, based on a debonding scenario, can be extracted from experimental results. One can assume that a good adhesion on PE probes is possible if $\tan\delta(\omega)/G' > 10^{-5}$ Pa^{-1} while a lower value [$\tan\delta(\omega)/G' > 0.5^{*}\,10^{-5}$ Pa^{-1}] is acceptable for adhesion on stainless steel.

Probe tack results are consistent with peel and shear results obtained with standard tests (Table 3). The higher shear resistance of HS4 is consistent with its low maximal extension during probe tack experiments at low debonding velocity (10 μm/s). Here, the increase in the cohesion does not result in an increase in the level of

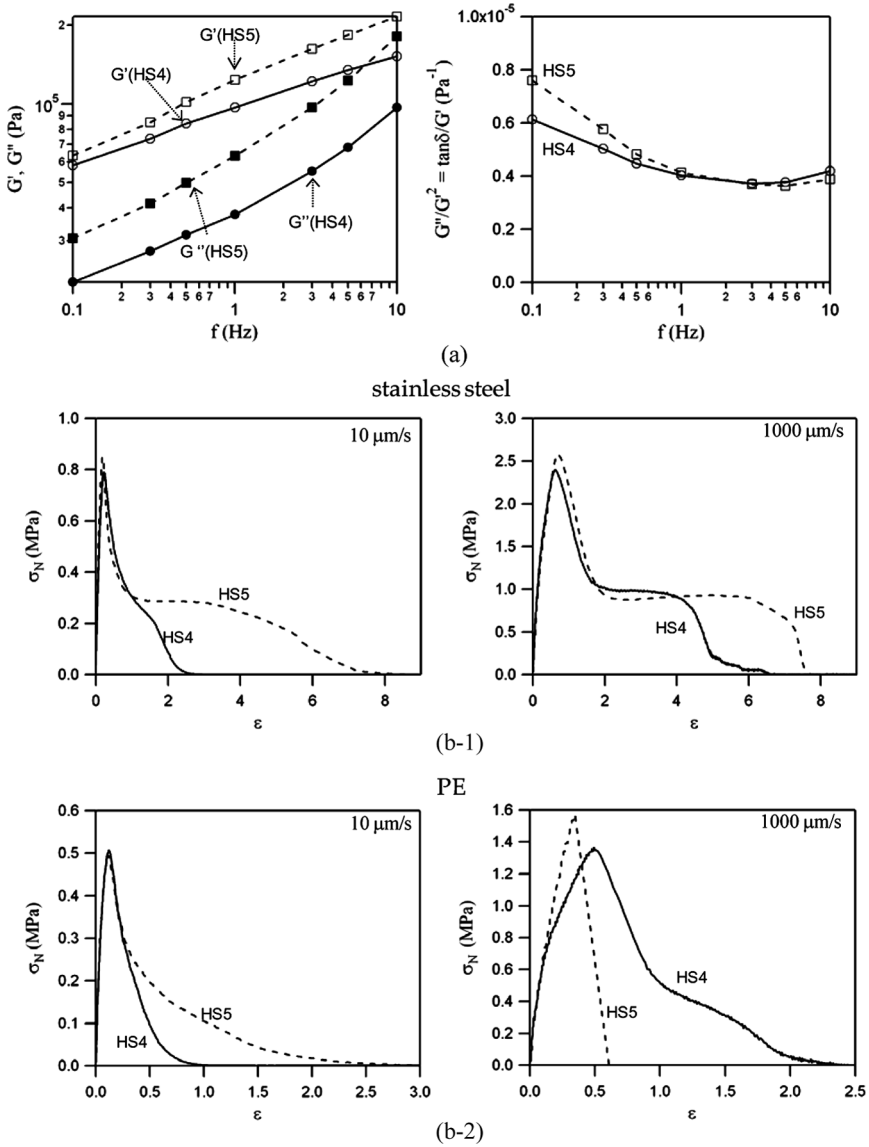

FIGURE 17 (1) Linear rheological results of two hard shell-soft core particles with different core T_gs and different amounts of CTA in their core. (Left) Evolution of elastic G' (empty symbols) and dissipative G'' (filled symbols) moduli as a function of the frequency. (Right) evolution of the ratio $\tan\delta/G'$. (2) Stress-strain tack curves: stainless steel probe and PE probe. Solid line: HS4, dashed line: HS5.

TABLE 3 Standard Adhesive Tests Results of HS4 and HS5

		HS4	HS5
Peel 24 h 180° (FTM1) (N/25 mm)	Glass	12.5 (10% CT[a])	14.65 (80% CT)
	HDPE plate	2.5	1.6
Shear (FTM8) (min)	Stainless steel (1 kg, 1 inch^2)	4448 CF[b]	1579 CF

[a]Cohesive transfer, *i.e.*, most of the adhesive remains on the adherend and is transferred from the backing.

[b]Cohesive failure, *i.e.*, adhesive remains on the steel and on the backing.

the fibrillation plateau but in a change of the debonding mechanism from a bulk mechanism with fibrillation to an interfacial mechanism, where cavities prefer to propagate at the interface between the probe and the adhesive layer.

The peel force of HS5 is higher than that of HS4 on a high energy surface such as glass while the opposite result is found on a lower energy surface such as PE. This is in agreement with tack results obtained at high debonding velocity (1000 μm/s) where the adhesive energy (area under the stress *vs*. strain curve) of HS5 was higher than that of HS4 on stainless steel and lower on PE.

From a more molecular design point of view, adhesive properties can be enhanced by an increase in the amount of CTA in the core (increasing dissipation). But then, the improvement in shear resistance requires an increase in the T_g of the shell. However, varying the T_g of an acrylic waterborne polymer by changing the copolymer composition also affects the gel fraction, the average molecular weights, and the level of branching. An alternative strategy is to activate an interfacial crosslinking reaction between the particles after the synthesis process, just prior to the drying of the film. This strategy is really interesting to adjust cohesion without having any major effect on the composition of the particles and, thus, to obtain a well controlled structure of the dry film. Such a change in crosslinking is much more apparent in large strains than in small strains and in the next section we will focus on the importance of nonlinear deformation properties to predict adhesive properties.

4.2. Use of Large Strain Deformation to Further Refine Particle Design for Adhesive Properties

Since the deformation of PSA is highly strain rate dependent, their large strain properties have to be studied at strain rates that are relevant for tack tests. The instantaneous strain rate in a tack test

is defined as $\dot{\varepsilon} = V_{deb}/h_0(1+\varepsilon)$, where V_{deb} and h_0 are the debonding speed and the initial thickness of the adhesive layer, respectively. During tensile experiments, $\dot{\varepsilon} = V_t/L_0(1+\varepsilon)$, with V_t and L_0 the stretching velocity and the initial distance between clamps, respectively. Films for adhesive tests being about 100 μm thick and for an initial distance between tensile clamps equal to 17 mm, we find that tensile experiments performed at a fixed velocity equal to V_t=50 mm/min have to be compared with tack tests performed at V_{deb}=10 μm/s. Only results on stainless steel will be presented, even though performance on PE is also dominated by the high strain behavior and mainly by the degree of viscoelastic softening at intermediate strains.

4.2.1. Activation of a Crosslinking Reaction at the Interface of Soft and Dissipative Particles

Maybe the most spectacular example of the relevance of the nonlinear properties is seen in the effect of the interparticle crosslinking process; this point is addressed elsewhere [47,48]. Figure 18 displays results obtained on uncrosslinked and crosslinked SS1 (in the latter case all DAAM groups of the shell are crosslinked). From Fig. 18a, linear rheological properties do not seem to be much affected by the activation of the interfacial crosslinking. The elastic modulus stays well below the Dahlquist critical value. Peak stresses of both materials are similar as a consequence of similar values of G'. $\mathrm{Tan}\delta/G'$ is in both cases superior to 10^{-5} Pa^{-1} and detachment never occurs through the interfacial propagation of the cavities.

However, clear differences are observable in the shape of tack stress-strain curves at higher strains (Fig. 18b) and these can only be explained by large strain tensile results. Indeed, contrary to small strain properties, nonlinear rheological properties seem to be significantly affected by the activation of the interfacial crosslinking. In the case of uncrosslinked particles, no local minimum in the reduced stress curve is observed (Fig. 18c). This is a signature of a liquid-like behavior: the tensile specimen does not break but flows at the end of the test. On the contrary, in the case of interfacially crosslinked particles, strain hardening appears and is responsible for the fracture of the tensile sample (no flow). Activating an interfacial crosslinking triggers a transition from a viscoelastic liquid behavior to a viscoelastic solid.

In an adhesion test, the liquid-like behavior of uncrosslinked core-shell particles leads to a cohesive debonding. This is visible since tack curves present a double fibrillation plateau and the material can really flow at very high strains [3,49]. On activating interfacial crosslinking, a progressive transition from cohesive to adhesive debonding is observed.

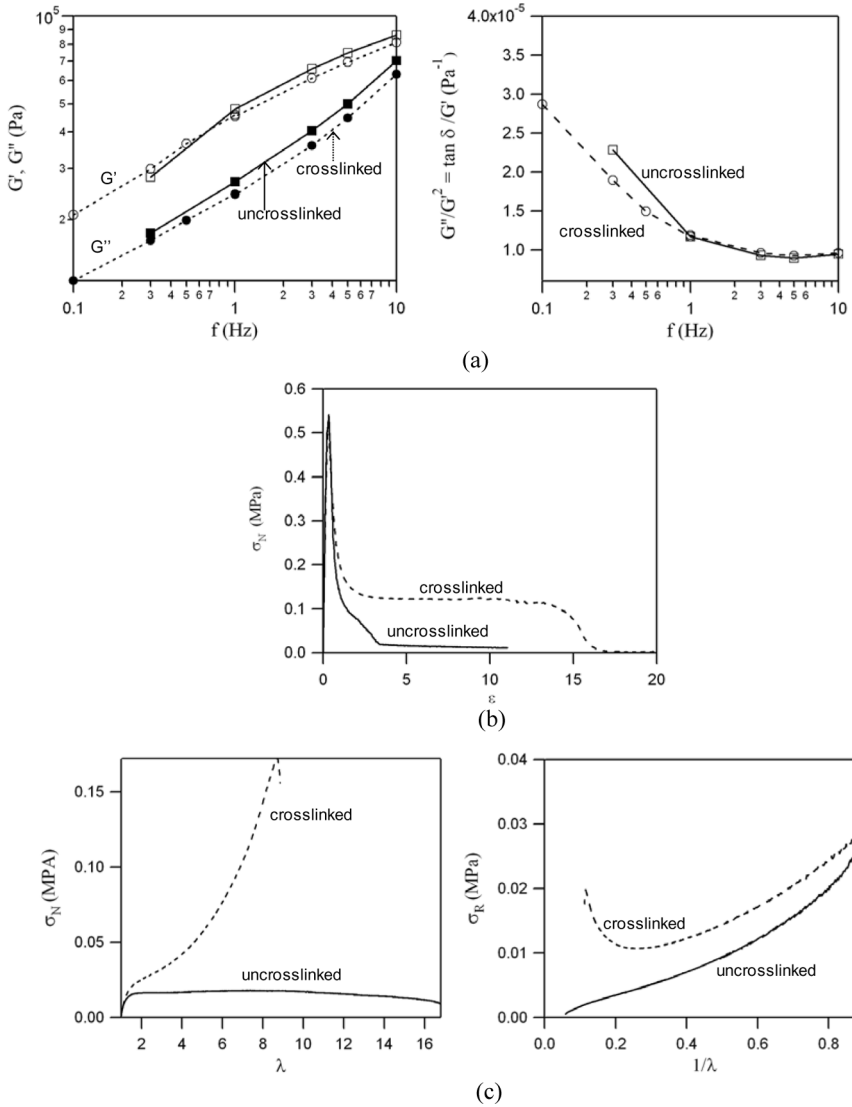

FIGURE 18 Effect of the activation of interfacial crosslinking of SS1 particles. Solid line: uncrosslinked particles (no ADH added), dashed line: interfacially crosslinked particles. (a) Linear rheology. (Left) evolution of the elastic G' (empty symbols) and dissipative G'' (filled symbols) moduli as a function of the frequency. (Right) Evolution of the ratio $\tan\delta/G'$; (b) Stress-strain tack curves. Tack experiments were performed at 10 μm/s on stainless steel; (c) Nonlinear rheology. (Left) Nominal stress *vs*. strain tensile curves. (Right) Mooney-Rivlin representations of tensile results.

It is at this stage interesting to note that crosslinked particles keep nearly the same value of C_2 indicating a similar density of temporary crosslinks while C_1, the density of permanent crosslinks, increases. This finally leads to a relatively high adhesion energy and an adhesive debonding rather than cohesive failure.

4.2.2. Influence of the Gel Content and the M_w of the Core

In the previous example it is clear that the introduction of a crosslinking chemistry in the shell has a profound effect on the large strain properties of the adhesive film. It is now interesting to investigate a change in the molecular architecture of the polymer in the core at a fixed degree of crosslinking of the shell. The first material studied (SS1) with 0.12 wt%/total polymer of CTA in the core was compared with a similar core-shell particle with 0.08 wt% of CTA (SS2) where all DAAM groups in the shell have been crosslinked by the ADH. The large strain behaviors of these two materials are displayed in Fig. 19. The overall shape of the curves is very similar. The cavitation stress is reached and the fibrillation process is initiated.

The parameter C_2 in the Mooney-Rivlin model is nearly the same for both materials, indicating that the density of non permanent crosslinks is nearly the same. However, C_1 increases without significant change in the position of the minimum along the $1/\lambda$ axis. This indicates a difference in the density of permanent crosslinks without any change in the percolating network determining the finite extensibility of the material.

An increase in the CTA amount in the core decreases the gel content and the M_w of the sol fraction (again, M_w decreases since the gel content is really low) of the core and, therefore, decreases the density of permanent crosslinks. This loss of cohesion is confirmed by the decrease in the fibrillation plateau level on stress-strain tack curves on both stainless steel and on PE (Fig. 19b). This could also be at the origin of the large increase in the length of the fibrillation plateau of SS1 compared with SS2. A more detailed explanation is proposed in the following paragraph.

As can be observed in Fig. 20, very often, the reduced stress *vs.* $1/\lambda$ curves cannot be easily fitted using the Mooney-Rivlin elastic model because there is no clear linear region of softening. To overcome this limitation, we decided to adapt the methodology to evaluate the softening in the Mooney representation: we took the slope of the line defined by the experimental points at $1/\lambda = 0.8$ (25% strain) and at the point where σ_R goes through a minimum and strain hardening starts $[1/\lambda = (1/\lambda)_{hard}]$. For each material, three to five tests were performed and, as can be seen in Fig. 20b, the results are highly reproducible except at low strains corresponding to the range of $1/\lambda$ values

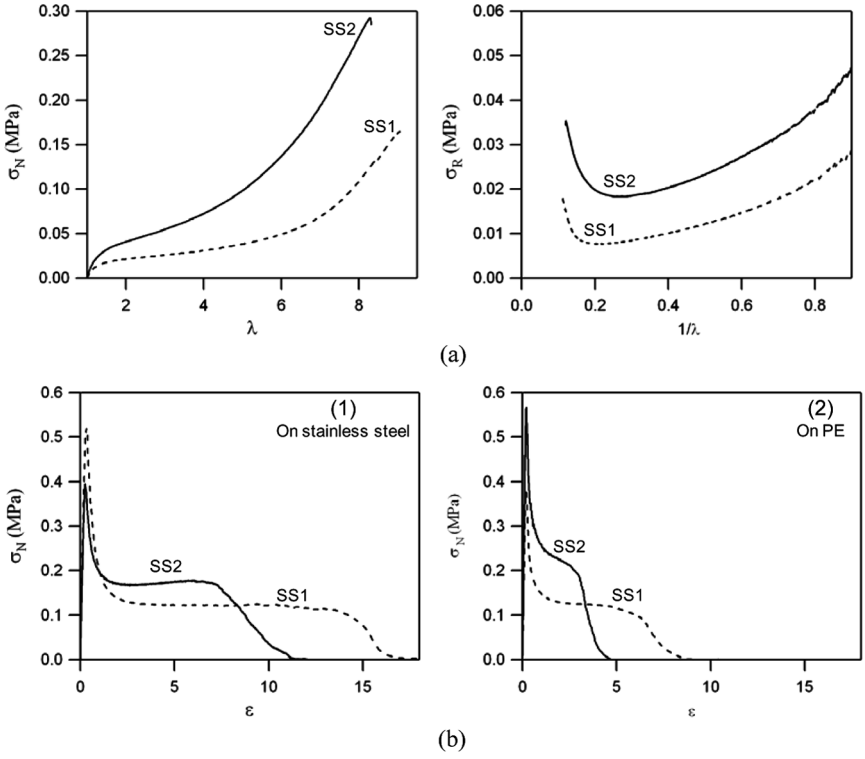

FIGURE 19 Effect of the amount of CTA in the core. Dashed line: crosslinked SS1, solid line: crosslinked SS2. [1] Nonlinear rheological results. (Left) Nominal stress *vs*. strain tensile curves. (Right): Mooney-Rivlin representations of tensile results. [2] Stress-strain tack curves. Tack experiments were performed on (a) stainless steel and on (b) PE at 10 μm/s.

above 0.8. That is why $1/\lambda = 0.8$ was chosen as the higher limit for the calculation of the slope. For an estimate of the contribution of the permanent crosslinks, we decided to take the value of the reduced stress when strain hardening starts and define it as C_{hard}. The crossover between the previously defined slope and y-axis has not been chosen since it lies sometimes in the negative range values. The slope between $1/\lambda = 0.8$ and the minimum in reduced stress will be called C_{soft}. In the case where no local minimum exists, C_{hard} is not defined and C_{soft} is calculated between $[0.8;\sigma_R(0.8)]$ and $[0.2;\sigma_R(0.2)]$. Usually a more dissipative material has many temporary crosslinks (that can relax) and much fewer permanent crosslinks, resulting in a high ratio of C_{soft}/C_{hard} and a long fibrillation plateau. Low values of C_{soft}/C_{hard}

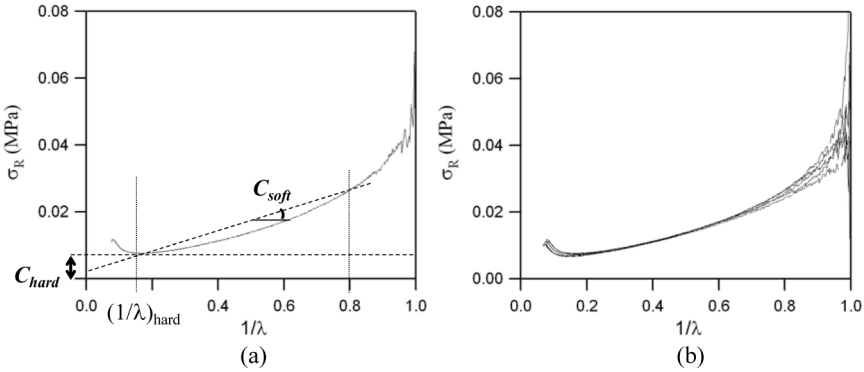

FIGURE 20 (a) Estimate of permanent and temporary crosslinks through C_{soft} and C_{hard}, respectively; (b) Five curves obtained on the same material are represented.

are, on the contrary, obtained in the case of more permanently crosslinked materials. In that case, the storage of elastic energy during elongation of the material is favored and leads to a rapid debonding of the adhesive layer when this energy is released.

Comparing SS1 and SS2, the maximal extension of the fibrils can effectively be predicted from this ratio C_{soft}/C_{hard}. An increase in the amount of CTA leads mainly to a decrease in C_{hard} without having much influence on C_{soft}.

Precise guidelines on the values of C_{soft}/C_{hard} clearly depend on the application. For the application that was considered with these interfacially crosslinked PSAs, which was adhesion on PE, a relatively high value of 3 was empirically determined as optimal by comparing adhesive tests results and tensile tests.

4.2.3. Comparison between a Viscoelastic Material and a More Elastic One

In our next example we compare nonlinear properties of a highly dissipative material made of interfacially crosslinked soft core-soft shell particles (SS2) with that of a more elastic adhesive film made of soft and independently crosslinked particles (WB). The more elastic the material the less pronounced is the softening. This is experimentally observed by the less steep slope of the reduced stress *vs.* $1/\lambda$ curve at intermediate strains (Fig. 21a).

If we consider again the ratio C_{soft}/C_{hard}, the longer fibrillation plateau of the core-shell particle is a consequence of both a decrease in the cohesion governed by permanent crosslinks and measurable

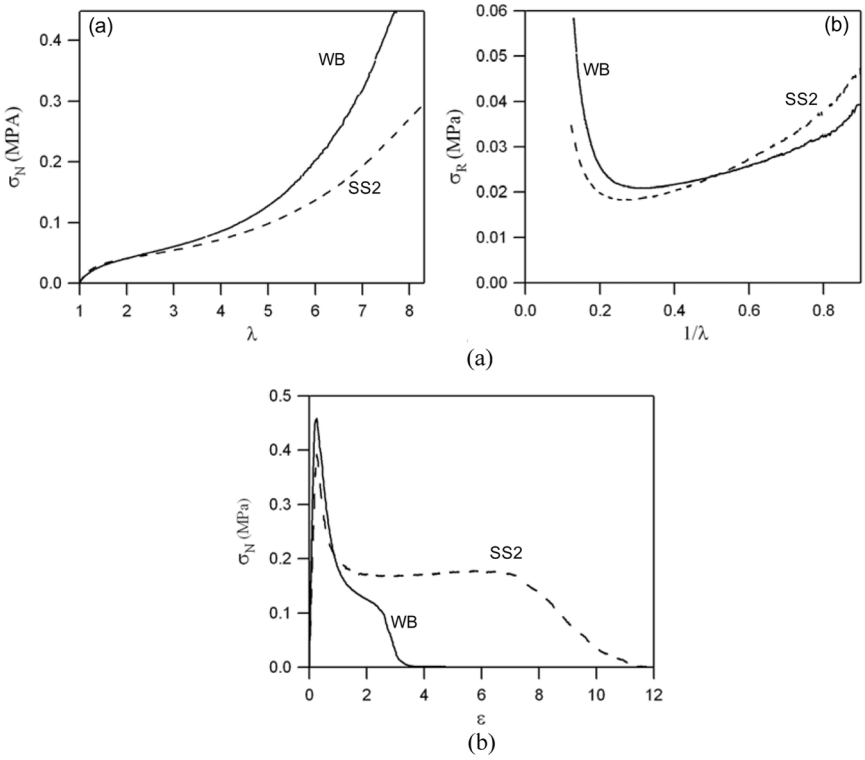

FIGURE 21 Comparison between an elastic material and a more viscoelastic one. Solid line: WB, dashed line: crosslinked SS2. [1] Nonlinear rheological results. (a) Stress-strain tensile curves; (b) Mooney-Rivlin representations of tensile results. [2] Stress-strain tack curves. Tack experiments were performed on stainless steel at 10 μm/s.

by C_{hard} (decrease from 0.021 to 0.019 MPa) and an increase in the dissipation measurable by C_{soft} (increase from 0.022 to 0.040 MPa). This finally leads to an increase in C_{soft}/C_{hard} from 1.05 to 2.11.

For adhesion on stainless steel (Fig. 21b) (the application considered here), a value of 2.11 for C_{soft}/C_{hard} was optimal. As discussed just above, for adhesion on PE, better adhesive properties can be obtained with higher values of C_{soft}/C_{hard}. This is an example of the coupling between surface and rheological properties.

In conclusion, the characterization and analysis of the nonlinear properties is really useful for the fine tuning of adhesive properties when the linear viscoelastic criteria are met. This has been already demonstrated by Roos and Creton [39] but what is especially new in

the present study is that the softening at intermediate strains is probably not much due to the elastic and reversible reorientation of entanglements but rather to their viscous and irreversible relaxation. This is due to the low entanglement density of acrylic polymers due to their high M_e [M_e of P(2EHA) varies between 35,000 to 130,000 g/mol and M_e of P(BA) varies between 17,000 and 26,000 g/mol [50]] and to the much more heterogeneous crosslinking of these acrylic systems relative to the physically crosslinked block copolymer-based PSA. Softening is then due to viscoelastic processes such as relaxation leading to viscous dissipation.

We have shown that the tensile tests can predict cohesive or adhesive debonding at the end of a tack experiment, as well as the level of stress at which a plateau in fibrillation is formed. The quantitative prediction of the detachment strain of the fibrils remains a difficult problem as it involves both nonlinear elasticity and linear viscoelasticity. An attempt to discuss this process has been recently proposed by Glassmaker *et al.* [35].

It is clear that other factors such as the average molecular weight between entanglements, M_e, or the surface energy, γ, of the adhesives will affect the adhesive performance. However, in this study we focused on the nonlinear rheology with polymeric systems where these two parameters (directly related to the average monomer composition) were kept relatively constant.

5. CONCLUDING REMARKS

A more refined methodology is proposed for the optimization of the adhesive properties of PSAs and is illustrated with examples taken from the particular case of core-shell particle morphology with a thin shell.

- First, the overall monomer composition of each phase has to be chosen in order to reach a T_g in the target for the adhesive application. Adhesion strongly depends on T_g and a maximum is reached between 50 and 70°C above the T_g[4].

A high shell T_g and a low core T_g can be obtained by increasing the concentration of hard monomers (such as styrene or MMA) in the shell and increasing the concentration of soft monomers (such as 2-EHA, EA, or BA) in the core.

- Linear rheological measurements can then be used to have a first idea of adhesive performance. Two important criteria must be fulfilled to obtain tackiness on a given surface.

1. $G' < 100\,\text{kPa}$. Higher values of G' lead to premature adhesive debonding due to a poor or incomplete contact during the bonding phase and to a lack of fibril formation.
2. $\mathcal{G}_c/G'(\omega)$ must be higher than a critical level to form a fibrillar structure. A linear viscoelastic approximation of $\mathcal{G}_c$ provides an approximate criterion for fibril formation:

$$\tan\delta(\omega)/G'(\omega) > 0.5^*/10^{-5}\ \text{Pa}^{-1} \text{ for steel or high energy surfaces}$$

$$\tan\delta(\omega)/G'(\omega) > 10^{-5}\ \text{Pa}^{-1} \text{ for PE or polyolefin surfaces.}$$

Crack propagation accompanied by a low adhesion energy is expected if this second criterion is not respected and this is either due to a too high elastic modulus or to a very low level of viscoelastic dissipation.

For our acrylic systems, an increase in $\tan\delta(\omega)$ can be obtained through the addition of CTA, specifically in the core, since the objective is to control adhesion and dissipation by the core. A concentration equal to about 0.1 wt%/total monomer seems to be an acceptable value which can be further optimized if necessary. However, other synthesis or formulation strategies can be used for the same purpose with other families of PSAs.

The linear viscoelastic properties are very useful to determine whether the PSA is too hard and adheres poorly. It fails, however, at predicting when the PSA is not cohesive enough, since it is based on tack and not on shear resistance.

Shear resistance is notoriously difficult to predict but we showed that the large strain behavior of the PSA can be used to detect cohesiveness. Tensile tests can be analyzed using the Mooney-Rivlin representation of reduced stress. Usable PSAs which combine viscoelastic dissipation and shear resistance will invariably show a softening behavior at intermediate strains (due to the viscoelastic relaxation of entanglements) and a hardening at large strains (due to the finite extensibility of the percolating network of chains). The balance between softening and hardening is an important descriptor of the PSA performance. We propose a general method to obtain an approximate evaluation of this balance by defining two constants, C_{hard} and C_{soft}, which represent, respectively, the minimum value of reduced stress and difference between the reduced stress at 25% strain and this minimum value. Any PSA should have a well defined C_{hard} and the values of both parameters are very sensitive to the network architecture and microstructure of the PSA and can detect small changes which would be invisible in linear rheology but which can greatly impact the adhesive properties and, in particular, the shear resistance.

For the core-shell system we clearly demonstrated the existence of two synthetic tools impacting the value of these two constants. If the core of the particle is made more dissipative (by adding CTA) this leads to a decrease in C_{hard} and mostly to an increase in C_{soft}. These effects lead to an increase in peel force and adhesion energy in probe tests.

If the material does not have a detectable C_{hard} or its value is so low that shear resistance is poor, an interfacial crosslinking between particles during the drying of the films proves to be a good way to increase cohesion without damaging peel performance. A crosslinking reaction between a crosslinkable monomer (attached to the base polymer) and a water-soluble crosslinker can for, example, be activated. Further increase in the cohesion can be finally achieved by increasing the gel content or the T_g of the shell. In more general terms, a synthesis strategy leading to a very dilute but percolating network of crosslinks will have little effect on the linear viscoelastic properties but ensure resistance to creep and adhesive debonding of the PSA.

ACKNOWLEDGMENTS

The authors would like to thank all the collaborators of the "Designed Nanoscale Heterogeneities for Controlling Waterborne Pressure-Sensitive-Adhesive Performance" (NsHAPe) project funded by the European Commission Sixth Framework Program (Contract No. NMP3-CT-2004-505442). We would like specifically to thank C. Lei from the University of Surrey for the AFM image of Figure 9.

REFERENCES

[1] Creton, C., *MRS Bulletin* **28**, 434–439 (2003).
[2] Satas, D. (Ed.) *Handbook of Pressure Sensitive Adhesive Technology*, (Van Nostrand Reinhold, New York, 1989).
[3] Lakrout, H., Creton, C., Ahn, D., and Shull, K. R., *Macromolecules* **34**, 7448–7458 (2001).
[4] Zosel, A., *Colloid Polym. Sci.* **263**, 541–553 (1985).
[5] Lindner, A., Lestriez, B. S. M., Brummer, R., Maevis, T., Lühmann, B., and Creton, C., *J. Adhes.* **82**, 267–310 (2006).
[6] Creton, C. and Fabre, P., Tack, in *The Mechanics of Adhesion*, D. A. Dillard and A. V. Pocius (Eds.) (Elsevier, Amsterdam, 2002). Vol. 1, pp. 535–576.
[7] Zosel, A., *Adv. Pressure Sensitive Adhes. Technol.* **1**, 92–127 (1992).
[8] Krenceski, M. A. and Johnson, J. F., *Polym. Eng. Sci.* **29**, 36–43 (1989).
[9] Jovanovic, R. and Dube, M. A., *Journal of Macromolecular Science-Polymer Reviews* **C44**, 1–51 (2004).
[10] Dos Santos, F. D. and Leibler, L., *Journal of Polymer Science Part B-Polymer Physics* **41**, 224–234 (2003).

[11] Aymonier, A., Papon, E., Castelein, G., Brogly, A., and Tordjeman, P., *J. Coll. Int. Sci.* **268**, 341–347 (2003).
[12] Aymonier, A., Ledercq, D., Tordjeman, P., Papon, E., and Villenave, J. J., *J. Appl. Polym. Sci.* **89**, 2749–2756 (2003).
[13] Aymonier, A., Papon, E., Villenave, J.-J., Tordjeman, P., Pirri, R., and Gérard, P., *Chem. Mater.* **13**, 2562–2566 (2001).
[14] Nase, J., Lindner, A., and Creton, C., *Phys. Rev. Lett.* **101**, 074503 (2008).
[15] Wang, T., Lei, C. H., Dalton, A. B., Creton, C., Lin, Y., Fernando, K. A. S., Sun, Y.-P., Manea, M., Asua, J. M., and Keddie, J. L., *Adv. Mater.* **18**, 2730–2734 (2006).
[16] Chang, E. P., *J. Adhes.* **34**, 189–200 (1991).
[17] Urahama, Y., *J. Adhes.* **31**, 47–58 (1989).
[18] Benyahia, L., Verdier, C., and Piau, J. M., *J. Adhes.* **62**, 45–73 (1997).
[19] Chiche, A., Zhang, W. H., Stafford, C. M., and Karim, A., *Measurement Science & Technology* **16**, 183–190 (2005).
[20] Kaelble, D. H., *Trans. Soc. Rheol.* **9**, 135–163 (1965).
[21] Shull, K. R. and Creton, C., *J. Polym. Sci. B Polym. Phys.* **42**, 4023–4043 (2004).
[22] Zosel, A., *J. Adhes.* **30**, 135–149 (1989).
[23] Zosel, A., *Adh. Age* **1989**, 42–47 (Oct. 1989).
[24] Lakrout, H., Sergot, P., and Creton, C., *J. Adhes.* **69**, 307–359 (1999).
[25] Poivet, S., Nallet, F., Gay, C., and Fabre, P., *Europhys. Lett.* **62**, 244–250 (2003).
[26] Yarusso, D. J., *The Journal of Adhesion* **70**, 299–320 (1999).
[27] Derail, C., Allal, A., Marin, G., and Tordjeman, P., *J. Adhes.* **61**, 123–157 (1997).
[28] Dahlquist, C. A., Pressure-Sensitive adhesives, in *Treatise on Adhesion and Adhesives*, R. L. Patrick (Ed.) (Dekker, New York, 1969), Vol. 2, pp. 219–260.
[29] Crosby, A. J., Shull, K. R., Lakrout, H., and Creton, C., *J. Appl. Phys.* **88**, 2956–2966 (2000).
[30] Creton, C. and Lakrout, H., *J. Polym. Sci. B Polym. Phys.* **38**, 965–979 (2000).
[31] Webber, R. E., Shull, K. R., Roos, A., and Creton, C., *Phys. Rev. E* **68**, 021805 (2003).
[32] Gent, A. N., *Langmuir* **12**, 4492–4496 (1996).
[33] Maugis, D. and Barquins, M., *J. Phys. D: Appl. Phys.* **11**, 1989–2023 (1978).
[34] Saulnier, F., Ondarcuhu, T., Aradian, A. and Raphael, E., *Macromolecules* **37**, 1067–1075 (2004).
[35] Glassmaker, N. J., Hui, C. Y., Yamaguchi, T., and Creton, C., *Eur. Phys. J. E* **25**, 253–266 (2008).
[36] Creton, C., Roos, A., and Chiche, A., Effect of the diblock content on the adhesive and deformation properties of PSAs based on styrenic block copolymers, in *Adhesion: Current Research and Applications*, W. G. Possart (Ed.) (Wiley-VCH, Weinheim, 2005), pp. 337–364.
[37] Good, R. J. and Gupta, R. K., *J. Adhes.* **26**, 13–36 (1988).
[38] Verdier, C. and Piau, J. M., *Journal of Polymer Science Part B-Polymer Physics* **41**, 3139–3149 (2003).
[39] Roos, A. and Creton, C., *Macromolecules* **38**, 7807–7818 (2005).
[40] Carelli, C., Déplace, F., Boissonnet, L., and Creton, C., *J. Adhes.* **83**, 491–505 (2007).
[41] Rubinstein, M. and Panyukov, S., *Macromolecules* **35**, 6670–6886 (2002).
[42] Brandrup, J. and Immergut, E. H., *Polymer Handbook* (Wiley, New York, 1999).
[43] Mallégol, J., Dupont, O., and Keddie, J. L., *Langmuir* **17**, 7022–7031 (2001).
[44] Chiche, A., Pareige, P., and Creton, C., *C. R. Acad. Sci. Paris, IV* **1**, 1197–1204 (2000).
[45] Chiche, A., Dollhofer, J., and Creton, C., *Eur. Phys. J. E* **17**, 389–401 (2005).

[46] Gacoin, E., Fretigny, C., Chateauminois, A., Perriot, A., and Barthel, E., *Tribology Letters* **21**, 245–252 (2006).
[47] Deplace, F., Rabjohns, M. A., Yamaguchi, T., Foster, A. B., Carelli, C., Lei, C. H., Ouzineb, K., Keddie, J. L., P. A. L., and Creton, C., *Soft Matter*. DOI: 10.1039/b15292f.
[48] Foster, A. B., Lovell, P. A., and Rabjohns, M. A., *Polymer*. DOI: 10.1016/j polymer.2009.01.054.
[49] Poivet, S., Nallet, F., Gay, C., Teisseire, J., and Fabre, P., *Eur. Phys. J. E* **15**, 97–116 (2004).
[50] Tobing, S. D. and Klein, A., *J. Appl. Polym. Sci.* **79**, 2230–2244 (2001).